FISEVIER

Contents lists available at ScienceDirect

Journal of Alloys and Compounds

journal homepage: www.elsevier.com/locate/jalcom



Evaluating the solid solution, local chemical ordering, and precipitation strengthening contributions in multi-principal-element alloys



Jia Li ^a, Xiaobao Fu ^a, Hui Feng ^a, Bin Liu ^b, Peter K. Liaw ^c, Qihong Fang ^{a,*}

- ^a State Key Laboratory of Advanced Design and Manufacturing for Vehicle Body, College of Mechanical and Vehicle Engineering, Hunan University; Changsha 410082, PR China
- ^b State Key Laboratory of Powder Metallurgy, Central South University; Changsha 410083, PR China
- ^c Department of Materials Science and Engineering, The University of Tennessee, Knoxville, TN 37996, USA

ARTICLE INFO

Article history:
Received 3 November 2022
Received in revised form 16 December 2022
Accepted 16 December 2022
Available online 21 December 2022

Keywords:
Random solid solution
Local chemical ordering
Precipitation
Strengthening mechanism
Mechanical property
Multi-principal-element alloy

ABSTRACT

Numerous theoretical and experimental studies suggest that the chemical ordering microstructure plays an important role for the strength and plastic deformation in the multi-principal-element alloy (MPEA). Despite the importance of this fact has been well confirmed, little is known about the influence of chemical ordering degree from the atomic scale to nano scale for the nanocrystal MPEA over a wide grain size range. In the present work, considering the abnormal local stacking fault energy originated from the heterogeneous chemical element concentration, the modified Hall-Petch relationship is elaborately established in MPEA, quite different from the traditional alloys. Additionally, the effects of the solid solution, local chemical ordering, and precipitation on the strengthening contribution and strain partition are evaluated. The increase of the chemical ordering degree improves the stacking fault energy and deformation gradient, as well as microrotation field. This trend leads to the yield strength owing to the formation of the slender shear bands. The geometry of the ordered structure is deformed and twisted to a certain extent, for the compatible plastic deformation. This work gives the atomic understanding of chemical-ordering-degree dominated strengthening mechanisms, to develop the strong and ductile MPEAs with desired properties. *Data availability statement:* The data that support the findings of this study are available from the corresponding author upon reasonable request.

© 2022 Elsevier B.V. All rights reserved.

1. Introduction

The local chemical short-range order (CSRO) invariably exists in the multi-principal-element alloy (MPEA) at low temperatures or after long-time annealing and affects the deformation behavior to enhance the mechanical properties [1–4]. Recently, the existence of CSRO structures in the CoCrNi MPEA has been directly confirmed by transmission electron microscopy (TEM) [5,6]. The coherency strain fields arising from CSRO structures suppress dislocation movement to increase the threshold stress in the Al0.3CoCrFeNi MPEA [7]. Moreover, the formation process of the local order structure, such as nanoclustering and nanoprecipitation, influences the concentration and distribution of elements around there, and a low stacking fault energy (SFE) fluctuation causes the full dislocation to split into wide partials, resulting in the occurrence of cross-slip at high stress levels [8,9].

* Corresponding author. E-mail address: fangqh1327@hnu.edu.cn (Q. Fang).

More recently, the results of molecular dynamics (MD) simulations reveal that the SRO-induced composite microstructure enhances both the ultimate strength and ductility [10]. The lattice distortion and CSRO play the key role in the nucleation and evolution of dislocations and nanotwins in the single crystal and nanocrystalline CoCrNi MPEA [11]. Compared with the random solid solution state sample, the average hardness in a stable SRO sample increases 13.7% due to the dislocation pinning induced by the local Ni-rich regions [12]. The degree of CSRO depends on the effective cooling rate in Zr45Cu45Ag10 metallic glass, and the regions of Cu-rich and Ag-rich have the obvious differences of the dynamic mechanical properties [13]. The CSRO leads to a softening of the BCC Co16.67-Fe36.67Ni16.67Ti30 MPEAs relative to the random solid solution state sample, duo to the low solid solution strengthening [14]. The formation of mechanically derived short-range order in a Fe40Mn40Cr10Co10 MPEA has a certain contribution to the vield strength, mechanical twinning, and deformation-induced transformation [15], and relies on the ordering degree/extent on the applied strain rates. The nanoindentation of the single crystal CoCrNi MPEA

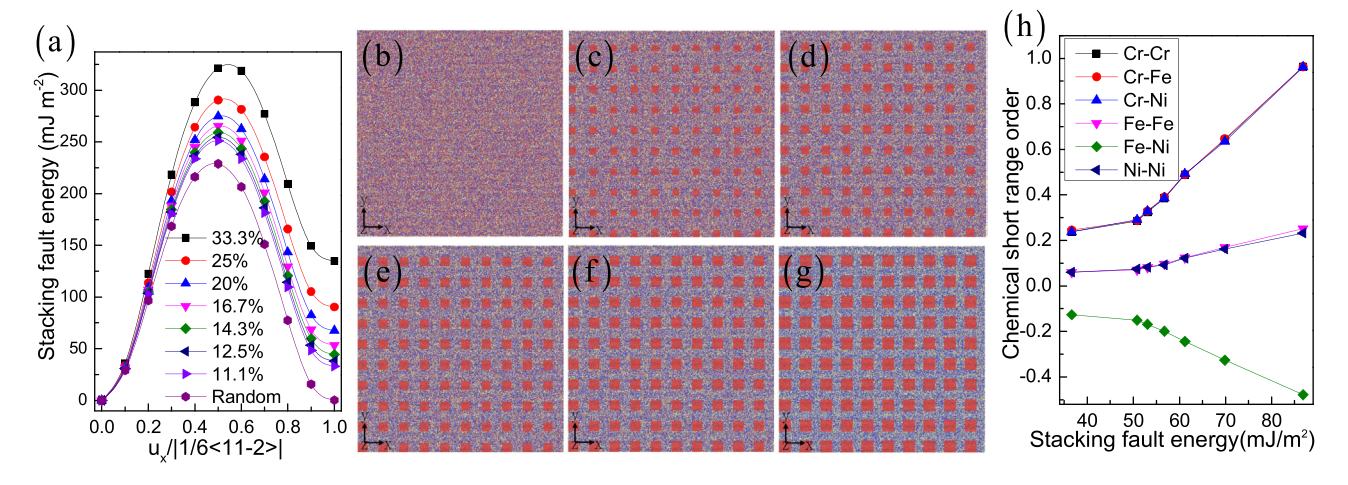


Fig. 1. The stacking fault energy with the increase of ordered structure fraction (a). The corresponding configurations include the random sample (b) and different ordered phase VFs of 11.1 (c), 16.7 (d), 20 (e), 25 (f), and 33.3 (g). The pairwise chemical short-range order parameters at different ordered phase VFs (h).

demonstrates that CSRO inhibits dislocation extension and cross-slip to enhance the hardness [16,17]. However, the influence of the random solid solution, local chemical ordering, and precipitation on the mechanical and physical behaviors are still far from being fully understood, especially for the nanocrystalline MPEA.

In this work, the effect of the local order structure on the deformation mechanisms and tensile behavior of the nanocrystalline FeCrNi MPEA are studied using atomic simulations. The CSRO degree correlated with the yielding strength is quantitatively analysed. Compared with the random solid solution state sample, the CSRO model exhibits higher strength in the nanocrystalline FeCrNi MPEA. The detailed microstructure and dislocation evolution are characterized, and the strain distribution is also considered. Here, the present work could provide an in-depth understanding of role of CSRO degree on the atomic-level deformation mechanisms.

2. Method

2.1. Material

The previous work shows the local element enrichment to result in the local chemical ordering [6,14,18,19]. Hence, the size of the Crelement enrichment region is 0, 1, 2, and 5 nm (Fig. 1b-g), which is used to regulate the degree of short-range order based on the result of the previous simulation and experiment [14,18,19]. Here, the corresponding volume fractions (VFs) of the ordered phases are 0 %, 11.1 %, 16.7 %, 20 %, 25 %, and 33.3 %. The size of sample is $89.9 \times 89.9 \times 2.5 \text{ nm}^3$, where the thickness of the columnar grain is larger than the cutoff distance of 5 Å for meeting the periodicity along the z direction. The nanocrystalline is built by the Voronoi method [20], and the average grain size is 5, 7, 10, 15, and 20 nm (See Fig. S1). The atomic number is about 1,720,000. The z direction is set along the < 111 > direction, and periodic boundary conditions are applying all directions [20]. To construct the desired MEA FeCrNi sample with the random elements, the atoms in the polycrystal Cr are randomly replaced by atoms of Fe, and Ni, as presented in Fig. 1b. To the MEA FeCrNi sample with local chemical ordering, the square Cr element segregation region is created in the MEA FeCrNi sample in Fig. 1c-g. Here, the nanostructured MEA FeCrNi film of three-dimensional (3D) < 111 > textured (or columnar) grains is built. Here, according to the size of the local ordered structure, we would divide the samples into three categories: random solid solution corresponding to the size less than 0.5 nm (size \leq 0.5 nm), local chemical ordering corresponding to the size less than 3 nm $(0.5 < \text{size} \le 3 \text{ nm})$,

and precipitation corresponding to the size less than 100 nm $(3 < \text{size} \le 100 \text{ nm})$.

2.2. Simulation detail

According to the Maxwell Boltzmann distribution, the velocities of all atoms are randomly set. Before the loading, the sample is first subjected to the energy minimization using the conjugate gradient method, and NVT dynamics (the canonical ensemble with a constant number of particles, volume and temperature) at the temperature of 300 K for 100 picoseconds in order to the relaxation. Then, NPT dynamics (the isothermal-isobaric ensemble with a constant number of particles, volume and pressure) at the temperature of 300 K is performed for 100 picoseconds in order to the further relaxation. A time step is 1 femtosecond. The uniaxial tensile loading with the constant rate of 1×10^8 s⁻¹ is applied along the x-direction under NPT dynamics at temperature of 300 K. The temperature in the NVT and NPT dynamics is adjusted by the Nose-Hoover method [20-22]. The maximum engineering strain reaches 6 %. An embedded-atom method potential [10,23-25] is employed to the interactions of atoms in the MPEA FeCrNi. The MD simulations are computed by the open-source Large-scale Atomic/Molecular Massively Parallel Simulator code [26]. The local atomic structure is analyzed by the common-neighbor analysis (CNA), and the microstructural evolution is presented via the Ovito software [27]. Based on the value of CNA, the green color represents face-centered cubic (fcc) structure, the red color stands for hexagonal close-packed (hcp) structure, and the blue color means other structure including dislocation, and grain boundary.

2.3. Chemical short range order parameter

It is common to describe SRO in form of Warren–Cowley short-range order or pair-correlation parameters which is defined as $\alpha_{ij}^m = \left(p_{ij}^m - C_j\right)/(\delta_{ij} - C_j)$ [28,29], where m means the mth nearest-neighbor shell of the central atom i, p_{ij}^m is the average probability of finding a j-type atom around an i-type atom in the mth shell, C_j is the average concentration of j-type atom in the system, and δ_{ij} is the Kronecker delta function. When $\alpha_{ij}^m = 0$, this feature describes random alloys namely in this case elements i and j are found in the alloy system. In the case of $\alpha_{ij}^m > 0$ there is a tendency of clustering or segregation of i-i and j-j pairs and for $\alpha_{ij}^m < 0$ there is a tendency of unlike pairs ordering i-j.

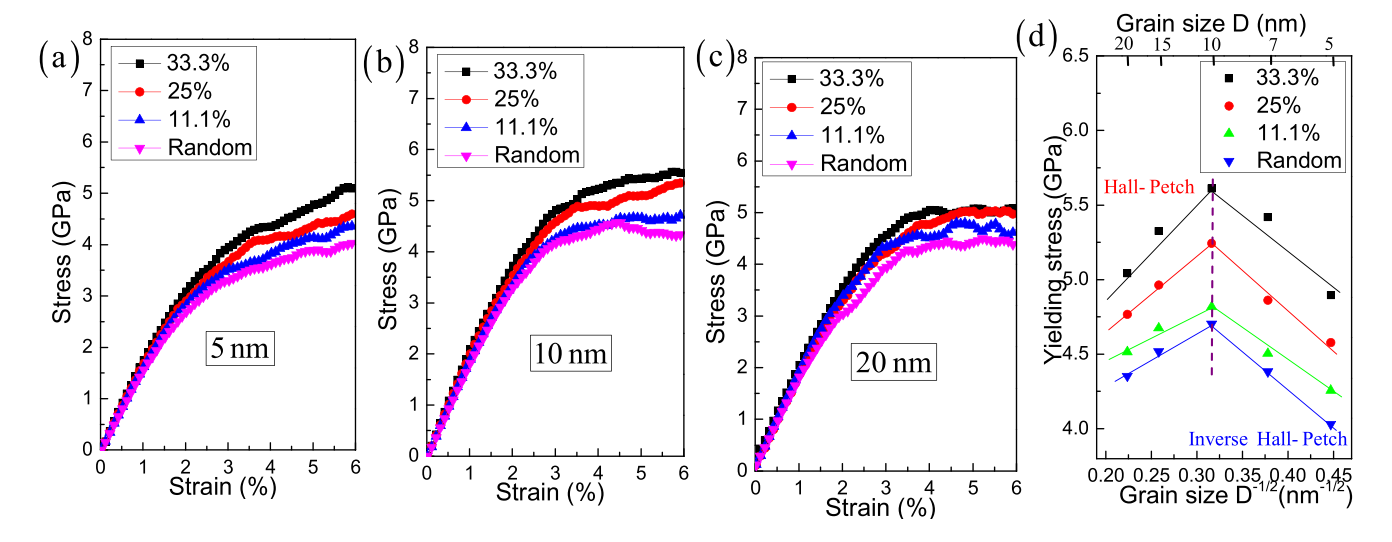


Fig. 2. The average stress-strain curves for different grain size samples (a-c). For each average grain size, the average stress-strain curve is obtained by averaging over three independent MD calculations (see Appendix A), for eliminating the errors caused by the grain shape artificially constructed. The relationship between the yielding strength and average grain size (d).

3. Results

3.1. Stacking fault energy

The deformation characteristics and mechanical behavior of materials are strongly dependent on the stacking-fault energy (SFE), which directly influences on the slip mode, and deformation twinning as well as phase transformation in the fcc alloys [30]. Thus, a basic understanding of how the SFE is affected by composition plays a crucial role in the alloy design. Here, for the sample with different sizes of the ordered structures, the SFE is presented in Fig. 1a, and the corresponding models are described in Fig. 1b-g. Here, the ordered structure fraction is 0 %, 11 %, and more than 16.7 %, which stands for the sample with random solid solution, the sample with local chemical ordering, and the sample with precipitation. The increased VF of an ordered phase would increase the SFE in equimolar multicomponent alloys. The SFE can change from 35 to 87 mJ/m² and would strongly affect the deformation behavior of the FeCrNi MPEA by controlling the nucleation and emission of the full dislocation and partial dislocation [31]. Hence, the variation of SFE with the degree of CSRO has the shape of a linear positive correlation (Fig. 1h).

3.2. Hall-Petch relationship

Fig. 2a-c show the tensile engineering stress-strain curves of our designed MEAs with different ordered phase VFs (0 %, 11.1 %, 25 %, and 33.3 %). In order to eliminate the difference of grain structures, the average stress-strain curve is calculated from 5 groups of independent samples. For the various average grain sizes, a yield strength increases with increasing the degree of local chemical ordering, but the flow stress after the yielding declines significantly. The MEAs with a random element distribution present a good tensile uniform elongation. The generalized form of the Hall-Petch relation can be expressed as $\sigma = \sigma_0 + kD^{-1/2}$ [32,33], where σ is the tensile flow stress, σ_0 is a friction stress, k is a constant which has been traditionally referred to as the Hall-Petch slope [34], and D is the average grain size. By fitting these three discrete yield strengths when the average grain size of d > 10 nm, the Hall-Petch relation of MEA can be expressed as: $\sigma = 3.5 + 3.7 \text{ D}^{-1/2}$ (0 %), $\sigma = 3.8 + 3.2 \text{ D}^{-1/2}$ (11.1 %), $\sigma = 3.6 + 5.1 \text{ D}^{-1/2}$ (25 %), and $\sigma = 3.7 + 6.1 \text{ D}^{-1/2}$ (33.3 %), as presented in Fig. 2d. For the average grain size of d < 10 nm, the inverse Hall-Petch relation of MEAs can be expressed as: $\sigma = 6.3-5.1$

Table 1 Elastic module for a grain size of 5 nm.

Ordered phase VF	C11 (GPa)	C12 (GPa)	C44 (GPa)	Poisson's ratio	μ (GPa)
0%	242.5	87.7	60.1	0.294	66.5
11.1%	252.0	90.0	63.4	0.291	69.9
25%	270.9	94.7	69.1	0.287	76.2
33.3%	286.2	98.9	73.6	0.285	81.1

Table 2 Elastic module for a grain size of 20 nm.

Ordered phase VF	C11 (GPa)	C12 (GPa)	C44 (GPa)	Poisson's ratio	μ (GPa)
0%	227.4	69.1	63.4	0.263	69.3
11.1%	239.4	72.4	66.7	0.262	73.0
25%	261.1	78.6	72.3	0.261	79.4
33.3%	279.4	83.5	76.7	0.261	84.6

 $D^{-1/2}$ (0 %), σ = 6.1–4.3 $D^{-1/2}$ (11.1 %), σ = 6.8–5.1 $D^{-1/2}$ (25 %), and σ = 7.4–5.5 $D^{-1/2}$ (33.3 %), as exhibited in Fig. 2d.

In the context of the previous work [34], the slope of the Hall-Petch relationships considering the effect of SFE can be expressed as $k=\frac{\mu b(\alpha-\beta\gamma_{SF})}{2\pi(1-\nu)}$, where bis the Burgers vector, v is the Poisson's ratio, μ is the shear modulus from Tables 1 and 2, α and β are dimensionally consistent constants, and γ_{SF} is the stacking fault energy. The value of Burger vector is taken as 0.3591 nm, based on the FCC lattice parameter obtained from XRD [35]. Hence, the present research correlates the complex relationships between the extent of CSRO and SFE as well as microstructures.

3.3. Evolution of microstructures

To reveal the ordered phase VF on the microstructure evolution, the defect structures with the increased local chemical ordering degree are performed when the plastic strain has reached about 4 % (Fig. 3a), and the evolution of the dislocation density is presented (Fig. 3b). As a result, there is an obvious difference in the grain boundary configuration and dislocation structures formed inside the crystal grain (Fig. 3a). For the mean grain sizes of 5 nm and 20 nm, the grain boundary maintains a relatively complete structure for the

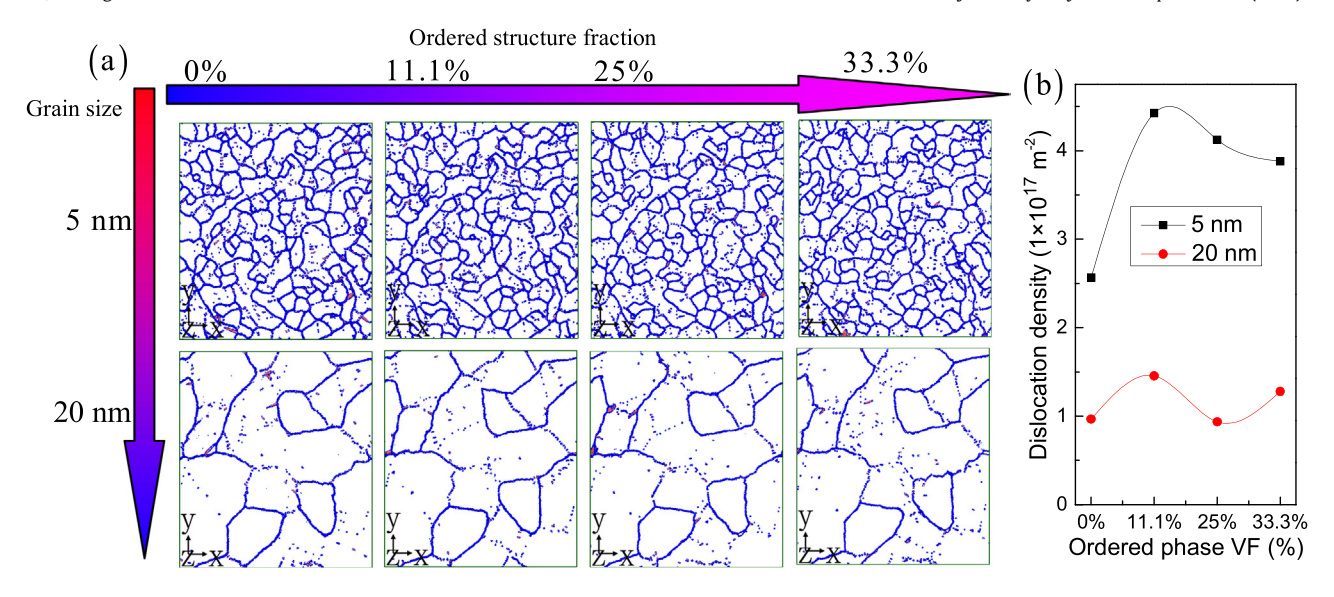


Fig. 3. Evolution of grain boundary structure and dislocation with the increased of the ordered phase VF for the grain sizes of 5 nm and 20 nm at the strain of 6% (a). The dislocation density with the increase of the ordered phase VF at the grain sizes of 5 nm and 20 nm (b).

sample with a random solid solution, and the existence of the ordered phase reduces the grain boundary stability (Fig. 3a) owing to the reduction of the grain boundary resistance in the low Cr matrix. This trend suggests that the limited amount of Cr solutes impacts the grain boundary stability at the large degree of local chemical ordering, in good agreement with those experimentally observed in nanocrystal FeCr alloys [36]. The dislocation density in the sample with an ordered phase increases in a comparison of the sample with random solid solution (Fig. 3b). For the inverse Hall-Petch relation, the increased ordered phase VF reduces the dislocation density. However, this result seems to be independent of the local chemical ordering degree in the Hall-Petch relation. For the large grain, the deformation of a grain boundary itself also plays a key role at the limited plastic deformation, which is not completely dependent on the dislocation slip mechanism. Thus, the increased ordered phase VF would not significantly disturb the evolution of the dislocation density.

The dislocation behavior plays a crucial role determining the strength and ductility of the materials [1,37,38]. Fig. 4(a) exhibits the

evolution of dislocation distribution with the increased CSRO degree at the strain of 6 %. Compared with other types of dislocations, a large number of Shockley partial dislocations occurs with the increase strain, which are responsible for the material plasticity. Quite a few stair-rod dislocations are generated, and maintain the work hardening of materials. It is widely known that the higher dislocation storage capacity represents better ductility in MPEAs [39,40]. Here, to analyse the influence of chemical ordering degree on the ductility of the FeCrNi MEAs, the variation of the mobile dislocation density with the increased strain is counted in Fig. 4(b), where the Shockley partial dislocations are mobile. For the high ordered phase VFs, increment of the mobile dislocation not only has a large number, but also has a fast multiplication rate. Thus, improving the CSRO degree is beneficial to enhance the ductility of MEAs.

4. Discussion

Fig. 5 shows a lattice distortion field generated in the ordered phase, where the high strain appears there within the grain

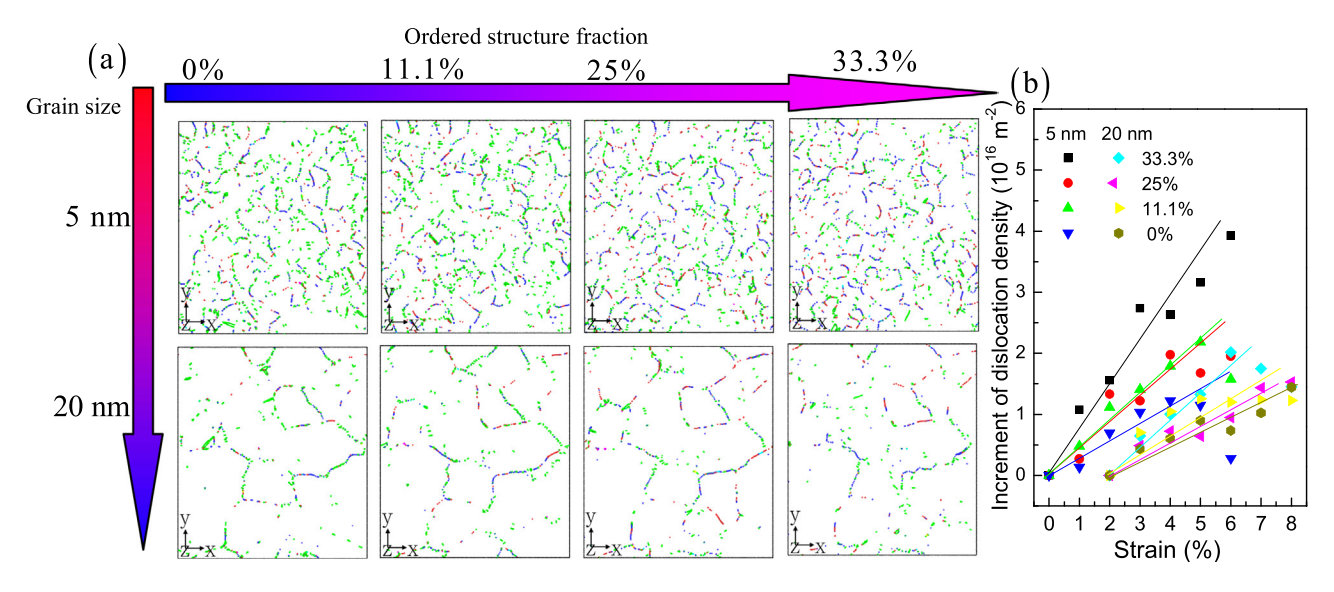


Fig. 4. Dislocation distribution with the increased of the ordered phase VF for the grain sizes of 5 nm and 20 nm at the strain of 6% (a). As indicated by the line colors, dislocations, including perfect dislocations (- ? blue line), Shockley partials (- ? green line), Hirth (- ? light-yellow), and stair-rod (- ? pink line) dislocations, have nonstandard Burgers vectors. Evolution of Shockley partial dislocation density with the increased strain for the grain sizes of 5 nm and 20 nm (b).

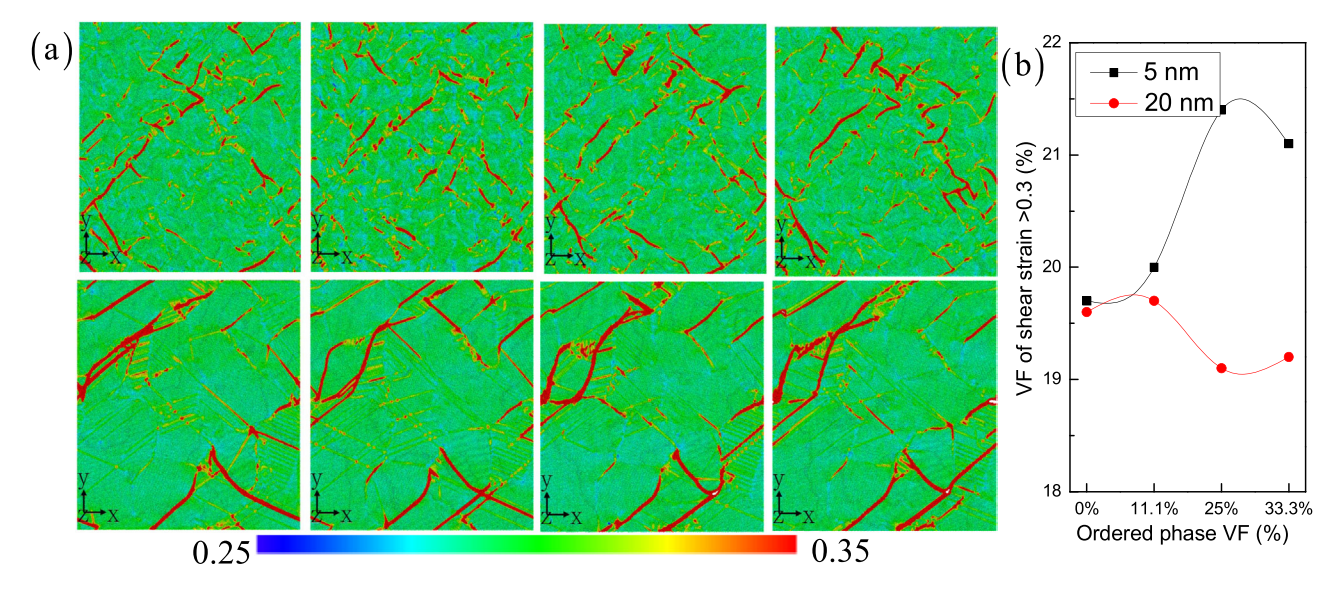


Fig. 5. The strain distribution at the grain sizes of 5 nm and 20 nm with the increased ordered phase VF (a). The VF of strain larger than 0.3 for the strain of 6% (b). The red atoms refer to the high strain region while blue atoms represent the low strain region.

boundary regions. The samples with low ordered phase VFs have some dense fine shear bands, and the slender shear bands exist with regions containing high ordered phase VFs. The increased ordered phase would change the morphology and distribution of shear bands for the grain sizes of 5 nm and 20 nm. Thus, the ordered phase plays a key role in influencing the strain partitioning for the same initial microstructure [41]. Hence, the solid solution, local chemical ordering, and precipitation produce the local lattice distortion to affect itself and its surrounding area. Fig. 6 presents the evolution of an ordered structure shape. The initially ordered phases with the same shape at different positions experiences the complex stress states, and tilt along various directions despite the uniaxial tensile deformation and the given grain. This phenomenon is quite different

from the well-known grain rotation during deformation [42], which is attributed to the glide of cross-grain dislocations and the grain-boundary-dissociation-induced dislocations (Fig. 3). Obviously, this process is difficult to be captured through the strain distribution. Besides, the coherency strain fields do not exist there around these nano-ordered structures which are different from the experimental observation for the huge increase in value of Hall-Petch slope [7]. Hence, we would analyze the deformation gradient and microrotation to reveal the effect of the ordered phase VF on the mechanical properties of the nanocrystalline MEA.

The lattice vectors for each atom are determined in both the reference and current configuration, and the deformation gradients for each individual atom can be calculated [43]. Fig. 7 shows the

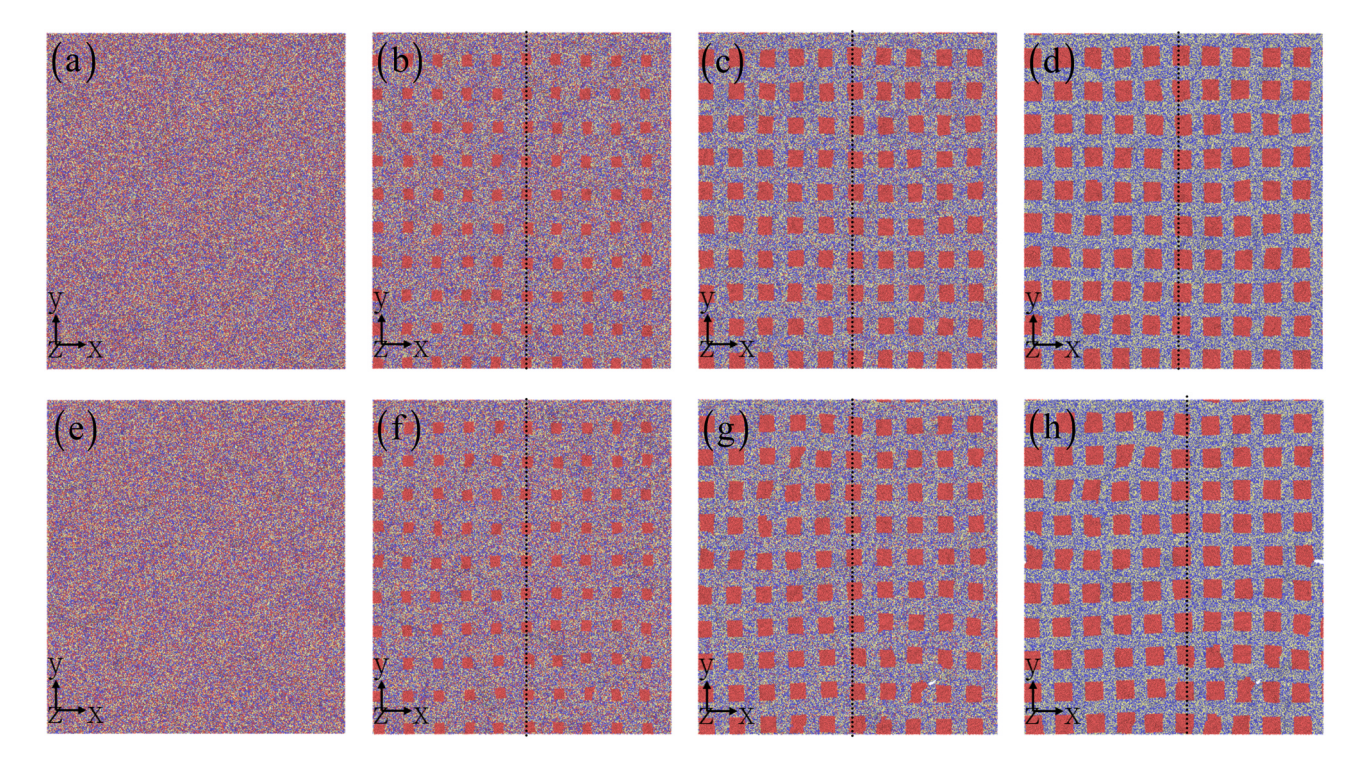


Fig. 6. The distribution of elements for the increased ordered phase VF at the strain of 6%. The grain size is 5 nm (a-d), and 20 nm (e-h). Here, the dotted line is used to better contrast the change of ordered phase.

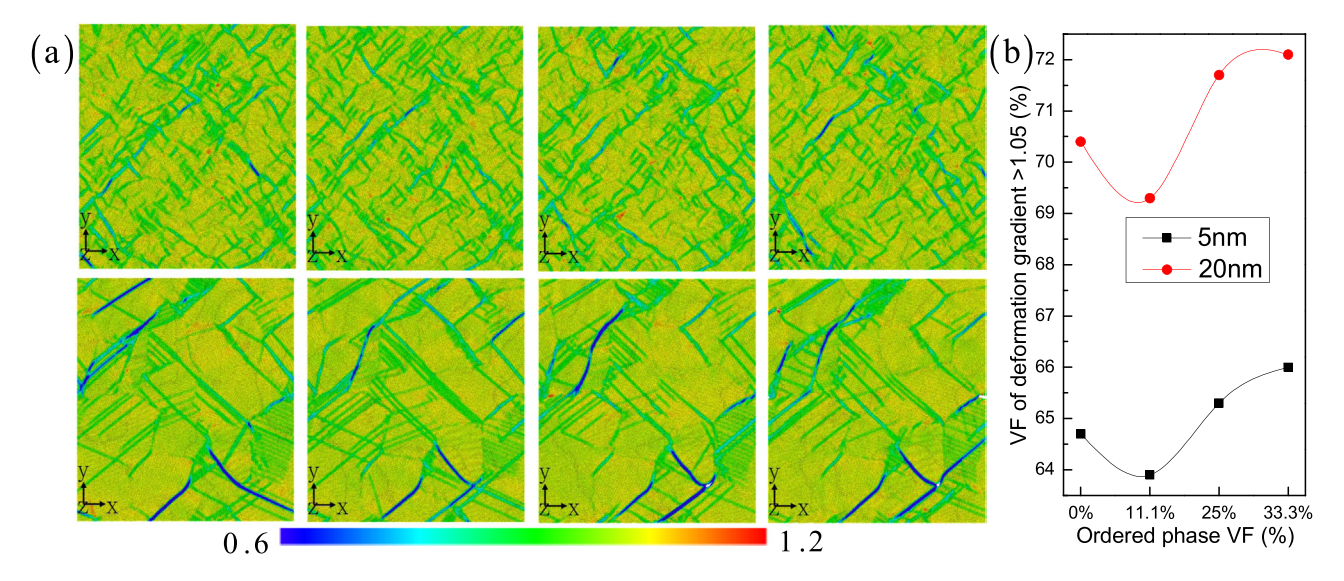


Fig. 7. The distribution of the deformation gradient along the x direction for the increase of the ordered phase VF at the strain of 6% (a). The VF of deformation gradient larger than 1.05 for the strain of 6% (b). The red atoms refer to the high deformation gradient region while blue atoms represent the low deformation gradient region.

deformation gradients at a strain of 6% for various ordered phase VFs. As well known, the dislocation nucleation and grain boundary movement could obviously reduce the elastic strain. In other word, the local plastic deformation reduces the elastic strain in regions with the increasing strain after yielding. For smaller grained samples, the deformation gradient can be displayed more clearly due to more plastic behavior activated (Fig. 7a). The large grain sample has a low deformation gradient induced by the weak grain boundary linkage characteristics. The increased ordered phase VF enhances not only the region size of low deformation gradient, but also the region size of high deformation gradient (Fig. 7b), where this case can be captured in nanocrystalline samples with grain sizes of 5 and 20 nm. This case would cause severely heterogeneous deformation, where the local region bears strong strain responses. It suggests that the heterogeneity of the atomic scale shear strain agrees with the shear strain gradient field (Figs. 5 and 7).

The previous work demonstrates that the microrotation is not only a useful measure for determining deformation [44,45], but also able to capture the nanoscale deformation (e.g., dislocation slip,

grain boundary sliding, and migration) [46]. Here, Fig. 8a shows the distribution of the microrotation fields along the z axis, where atoms are colored according to the calculated microrotation. Interestingly, some regions show an obvious microrotation even where high strain is absent. Furthermore, the microrotation fields surrounding the ordered phase (Fig. 8a) are strikingly similar to those shown in Fig. 7a. To further evaluate the distinct information regarding the deformation history of each atom from the microrotation, Fig. 8b exhibits the VF of the average atomic microrotation larger than 0.1 as a function of ordered phase VF for the increased imposed strain. The value of atomic microrotation shows an opposite trend over the increased ordered phase VF. Hence, the good strength and ductility of the nanocrystalline MEA is controlled by the complex restrictionand-regulation mechanism among the strain, deformation gradient, and microrotation fields dependent on the degree of chemical ordering.

To evaluate competitive relationships between the solid solution strengthening and the ordered structure strengthening, Fig. 9 shows the interaction between the dislocation and ordered solid solution

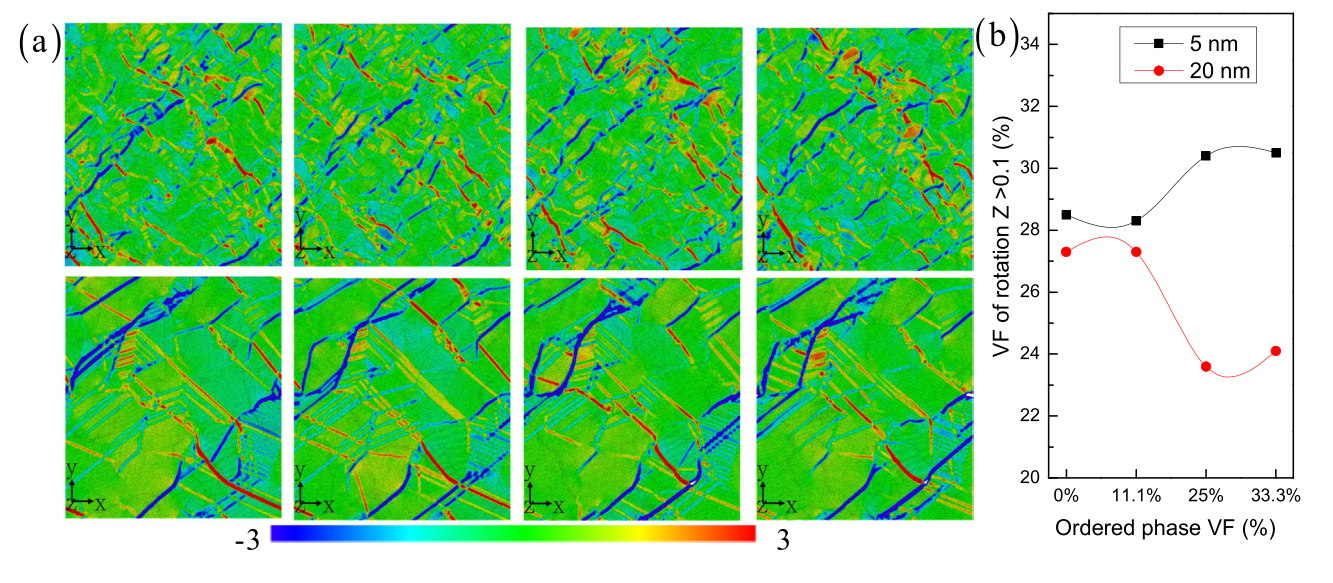


Fig. 8. The distribution of microrotation field along the z axis for the increase of the ordered phase VF at the strain of 6% (a). The VF of microrotation field larger than 0.1 for the strain of 6% (b). The red atoms refer to the region of high microrotation in a clockwise direction while blue atoms represent the region of high microrotation in a anticlockwise direction

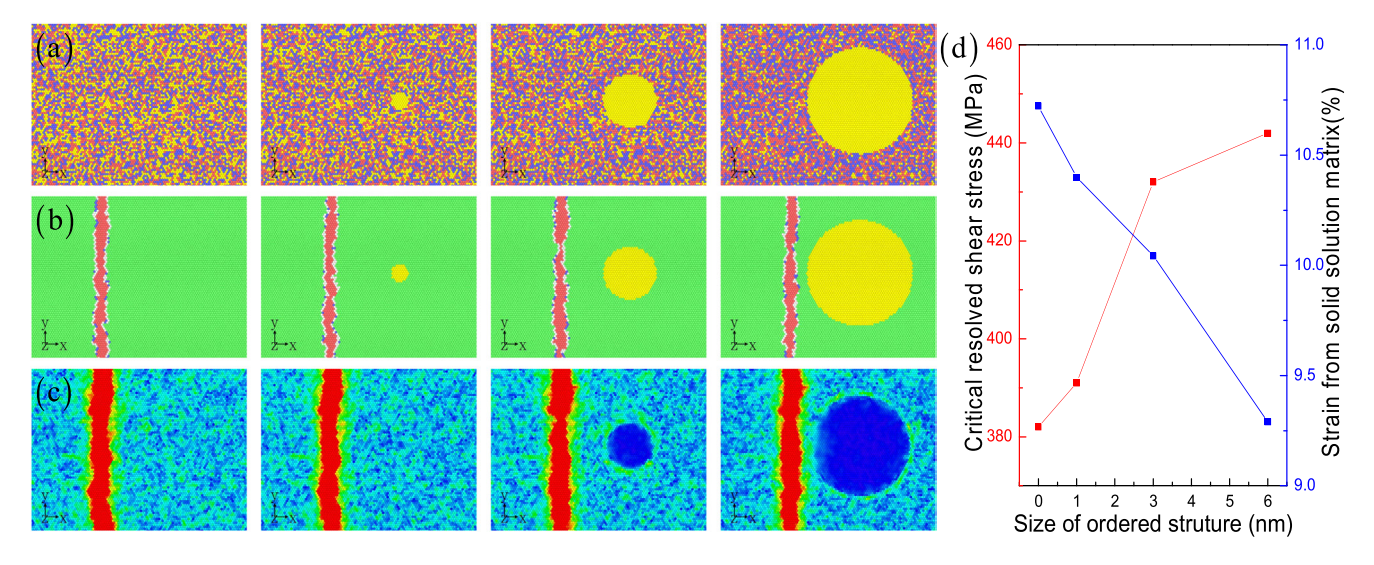


Fig. 9. The interaction of defect and ordered solid solution phase. The element distribution (a), the evolution of microstructure (b), and the strain distribution (c). The evolution of critical stress and strain with the increase of the ordered structure size (d).

phase. As the size of the Cr-riched ordered structure increases, the Cr content of the matrix decreases significantly (Fig. 9a). This trend would slightly affect the microstructure (Fig. 9b), which would not dominate the strengthening behavior of materials. It is worth noting that the low strain local regions markedly increase (Fig. 9c), thus reducing the solid solution strengthening from the contribution of lattice mismatch. The corresponding strain statistical results are presented in Fig. 9d, in consistent with the strain distribution (Fig. 9c). Hence, with the increase of the ordered structure size, the solution strengthening decreases, but the ordered strengthening increases (Fig. 9d). In order to obtain the highest strength, the reasonable strategy of the chemical element distribution mediated deformation/strain partitioning could be one of the most critical choice through the regulation of the ordered phase degree [47]. Furthermore, this composition distribution regulation could also be extended to the amorphous alloys. For example, based on the new strategy of gradient design of alloying compositions, the CuZr-based metallic glasses exhibit high strength and good ductility due to the mechanistic strain gradient effect [48], which affects the activation mechanisms of shear band nucleation and propagation. Hence, the introduction of short-range order is bound to produce the good ductility in amorphous alloys [49], via the rational distribution of local high strain to reduce the strain localization degree.

5. Conclusions

Considering a wide range of grain sizes, the deformation mechanisms of the nanocrystalline samples with different ordered phase degrees are investigated using atomistic simulations under the uniaxial tension at room temperature. The results show that the coherency strain fields do not exist there around these nano-ordered structures which are different from experimental observation for the huge increase in the value of the Hall-Petch slope. The local plastic deformation reduces the elastic strain with the increased strain after yielding. For a smaller grained sample, the deformation gradient in the small grain sample is displayed more clearly due to more plastic behavior activated, and the large grain sample has a low deformation gradient induced by the weak grain boundary linkage characteristics. The increased ordered phase VF enhances not only the region size of a low deformation gradient, but also the region size of a high deformation gradient. The heterogeneity of the atomic scale shear strain agrees with the shear strain gradient field. In addition, the good mechanical properties of the nanocrystalline MEA are controlled by the complex restriction-and-regulation mechanism among the strain, deformation gradient, and microrotation fields dependent on the degree of the chemical ordering. The present study provides an insight into the nanoscale deformation mechanism of the complex structured MPEAs, and motivates further intensively microstructure design by experiment.

CRediT authorship contribution statement

Jia Li: Formal analysis, Conceptualization, Writing - original draft, Supervision, Writing - review & editing, **Xiaobao Fu:** Formal analysis, Software, Methodology, **Hui Feng:** Formal analysis, Visualization, Supervision, **Bin Liu:** Formal analysis, Validation, Supervision, **Peter K. Liaw:** Formal analysis, Methodology, Writing - review & editing, **Qihong Fang:** Formal analysis, Conceptualization, Supervision, Project administration, Writing - review & editing.

Data availability

Data will be made available on request.

Declaration of Competing Interest

The authors declare that they have no known competing financial interests or personal relationships that could have appeared to influence the work reported in this paper.

Acknowledgments

The authors would like to deeply appreciate the supports from National Natural Science Foundation of China (U2267252, 12172123, and 12072109), Natural Science Foundation of Hunan Province (2022]J20001 and 2021JJ40032), The Science and Technology Innovation Program of Hunan Province (2022RC1200), and Natural Science Foundation of Changsha City (kq2202139). PKL very much appreciates the supports from (1) the National Science Foundation (DMR-1611180 and 1809640) and (2) the US Army Research Office (W911NF-13-1-0438 and W911NF-19-2-0049).

Appendix A. Supporting information

Supplementary data associated with this article can be found in the online version at doi:10.1016/j.jallcom.2022.168521.

References

- [1] Z. Lei, X. Liu, Y. Wu, H. Wang, S. Jiang, S. Wang, X. Hui, Y. Wu, B. Gault, P. Kontis, D. Raabe, L. Gu, Q. Zhang, H. Chen, H. Wang, J. Liu, K. An, Q. Zeng, T.G. Nieh, Z. Lu, Enhanced strength and ductility in a high-entropy alloy via ordered oxygen complexes, Nature 563 (2018) 546–550.
- [2] Q. Pan, L. Zhang, R. Feng, Q. Lu, K. An, A.C. Chuang, J.D. Poplawsky, P.K. Liaw, L. Lu, Gradient cell-structured high-entropy alloy with exceptional strength and ductility, Science 374 (2021) 984–989.
- [3] J. Ding, Q. Yu, M. Asta, R.O. Ritchie, Tunable stacking fault energies by tailoring local chemical order in CrCoNi medium-entropy alloys, Proc. Natl. Acad. Sci. USA 115 (36) (2018) 8919–8924.
- [4] J. Wang, P. Jiang, F. Yuan, X. Wu, Chemical medium-range order in a medium-entropy alloy, Nat. Commun. 13 (2022) 1021.
- [5] R. Zhang, S. Zhao, J. Ding, Y. Chong, T. Jia, C. Ophus, M. Asta, R.O. Ritchie, A.M. Minor, Short-range order and its impact on the CrCoNi medium-entropy alloy, Nature 581 (2020) 283–287.
- [6] X.F. Chen, Q. Wang, Z.Y. Cheng, M.L. Zhu, H. Zhou, P. Jiang, L.L. Zhou, Q.Q. Xue, F.P. Yuan, J. Zhu, X.L. Wu, E. Ma, Direct observation of chemical short-range order in a medium-entropy alloy, Nature 592 (2021) 712–716.
- [7] A. Jagetia, M. Nartu, S. Dasari, A. Sharma, B. Gwalani, R. Banerjee, Ordering-mediated local nano-clustering results in unusually large Hall-Petch strengthening coefficients in high entropy alloys, Mater. Res. Lett. 9 (2020) 213–222.
- [8] Q. Ding, Y. Zhang, X. Chen, X. Fu, D. Chen, S. Chen, L. Gu, F. Wei, H. Bei, Y. Gao, M. Wen, J. Li, Z. Zhang, T. Zhu, R.O. Ritchie, Q. Yu, Tuning element distribution, structure and properties by composition in high-entropy alloys, Nature 574 (2019) 223–227.
- [9] S. Yin, Y. Zuo, A. Abu-Odeh, H. Zheng, X.G. Li, J. Ding, S.P. Ong, M. Asta, R.O. Ritchie, Atomistic simulations of dislocation mobility in refractory highentropy alloys and the effect of chemical short-range order, Nat. Commun. 12 (2021) 4873.
- [10] S. Chen, Z.H. Aitken, S. Pattamatta, Z. Wu, Z.G. Yu, D.J. Srolovitz, P.K. Liaw, Y.W. Zhang, Simultaneously enhancing the ultimate strength and ductility of high-entropy alloys via short-range ordering, Nat. Commun. 12 (2021) 4953.
- [11] W.R. Jian, Z. Xie, S. Xu, Y. Su, X. Yao, I.J. Beyerlein, Effects of lattice distortion and chemical short-range order on the mechanisms of deformation in medium entropy alloy CoCrNi, Acta Mater. 199 (2020) 352–369.
- [12] X. Yang, Y. Xi, C. He, H. Chen, X. Zhang, S. Tu, chemical short-range order strengthening mechanism in CoCrNi medium-entropy alloy under nanoindentation, Scr. Mater. 209 (2022) 114364.
- [13] C. Tang, C.H. Wong, Formation of chemical short range order and its influences on the dynamic/mechanical heterogeneity in amorphous Zr–Cu–Ag alloys: a molecular dynamics study, Intermetallics 70 (2016) 61–67.
- [14] E. Antillon, C. Woodward, S.I. Rao, B. Akdim, Chemical short range order strengthening in BCC complex concentrated alloys, Acta Mater. 215 (2021) 117012
- [15] J.B. Seol, W.S. Ko, S.S. Sohn, M.Y. Na, H.J. Chang, Y.U. Heo, H.S. Kim, Mechanically derived short-range order and its impact on the multi-principal-element alloys, Nat. Commun. 13 (2022) 1–13.
- [16] Y. Xi, X. Yang, X. Yin, X. Liu, X. Zhang, H. Chen, Simultaneous strengthening effect of local chemical ordering and twin boundary on the medium entropy alloy CoCrNi, J. Alloy. Comp. 935 (2023) 168093.
- [17] S. Ma, J. Zhang, B. Xu, Y. Xiong, W. Shao, S. Zhao, Chemical short-range ordering regulated dislocation cross slip in high-entropy alloys, J. Alloy. Compd. 911 (2022) 165144.
- [18] Q.J. Li, H. Sheng, E. Ma, Strengthening in multi-principal element alloys with local-chemical-order roughened dislocation pathways, Nat. Commun. 10 (2019) 3563.
- [19] S. Dasari, A. Jagetia, A. Sharma, M.S.K.K.Y. Nartu, V. Soni, B. Gwalani, S. Gorsse, R. Banerjee, Tuning the degree of chemical ordering in the solid solution of a complex concentrated alloy and its impact on mechanical properties, Acta Mater. 212 (2021) 116938.
- [20] L. Li, H. Chen, Q. Fang, J. Li, F. Liu, Y. Liu, P.K. Liaw, Effects of temperature and strain rate on plastic deformation mechanisms of nanocrystalline high-entropy alloys, Intermetallics 120 (2020) 106741.
- [21] L.A. Zepeda-Ruiz, A. Stukowski, T. Oppelstrup, V.V. Bulatov, Probing the limits of metal plasticity with molecular dynamics simulations, Nature 550 (2017) 492.
- [22] X. Ke, J.C. Ye, Z.L. Pan, J. Geng, M.F. Besser, D.X. Qu, A. Caro, J. Marian, R.T. Ott, Y.M. Wang, F. Sansoz, Ideal maximum strengths and defect-induced softening in nanocrystalline- nanotwinned metals, Nat. Mater. 18 (2019).
- [23] W.M. Choi, Y.H. Jo, S.S. Sohn, S. Lee, B.J. Lee, Understanding the physical metallurgy of the CoCrFeMnNi high-entropy alloy: an atomistic simulation study, npj Comput. Mater. 4 (2018) 1–9.

- [24] Q. Fang, Y. Chen, J. Li, C. Jiang, B. Liu, Y. Liu, P.K. Liaw, Probing the phase transformation and dislocation evolution in dual-phase high-entropy alloys, Int. J. Plast, 114 (2019) 161–173.
- [25] Y. Tang, D.Y. Li, Dynamic response of high-entropy alloys to ballistic impact, Sci. Adv. 8 (2022) eabp9096.
- [26] S. Plimpton, Fast parallel algorithms for short-range molecular dynamics, J. Comp. Phys. 117 (1995) 1–19.
- [27] A. Stukowski, Visualization and analysis of atomistic simulation data with OVITO-the open visualization tool, Model. Simul. Mater. Sci. Eng. 18 (2009) 015012
- [28] D. Fontaine, The number of independent pair-correlation functions in multi-component systems, J. Appl. Crystallogr 4 (1971) 15–19.
- [29] J.M. Cowley, An approximate theory of order in alloys, Phys. Rev. 7 (1950) 669–675.
- [30] P.J. Ferreira, P. Müllner, A thermodynamic model for the stacking-fault energy, Acta Mater. 46 (1998) 4479–4484.
- [31] Z. Zhang, H. Sheng, Z. Wang, B. Gludovatz, Z. Zhang, E.P. George, Q. Yu, S.X. Mao, R.O. Ritchie, Dislocation mechanisms and 3D twin architectures generate exceptional strength-ductility-toughness combination in CrCoNi medium-entropy alloy, Nat. Commun. 8 (2017) (14390).
- [32] E.O. Hall, The deformation and ageing of mild steel: III discussion of results, Proc. Phys. Soc. B 64 (1951) 747–753.
- [33] N.J. Petch, The cleavage strength of polycrystals, J. Iron Steel Inst. 174 (1953) 25–28.
- [34] S. Wang, L.E. Murr, Effect of prestrain and stacking-fault energy on the application of the Hall-Petch relation in fcc metals and alloys, Metallography 13 (1980) 203–224.
- [35] M. Schneider, G. Laplanche, Effects of temperature on mechanical properties and deformation mechanisms of the equiatomic CrFeNi medium-entropy alloy, Acta Mater. 204 (2021) 116470.
- [36] X. Zhou, X.X. Yu, T. Kaub, R.L. Martens, G.B. Thompson, Grain boundary specific segregation in nanocrystalline Fe(Cr), Sci. Rep. 6 (2016) (34642).
- [37] H. Li, H. Zong, S. Li, S. Jin, Y. Chen, M.J. Cabral, B. Chen, Q. Huang, Y. Chen, Y. Ren, K. Yu, S. Han, X. Ding, G. Sha, J. Lian, X. Liao, E. Ma, J. Sun, Uniting tensile ductility with ultrahigh strength via composition undulation, Nature 604 (2022) 273–279.
- [38] J. Li, Y. Chen, Q. He, X. Xu, H. Wang, C. Jiang, C.T. Liu, Heterogeneous lattice strain strengthening in severely distorted crystalline solids, Proc. Natl. Acad. Sci. USA 119 (2022) e2200607119.
- [39] S. Picak, J. Liu, C. Hayrettin, W. Nasim, D. Canadinc, K. Xie, I. Karaman, Anomalous work hardening behavior of Fe40Mn40Cr10Co10 high entropy alloy single crystals deformed by twinning and slip, Acta Mater. 181 (2019) 555–569.
- [40] W. Jiang, H. Wang, Z. Li, Y. Zhao, Enhanced mechanical properties of a carbon and nitrogen co-doped interstitial high-entropy alloy via tuning ultrafine-grained microstructures, J. Mater. Sci. Technol. 144 (2023) 128–137.
- [41] T.F. Zheng, J.C. Lv, Y. Wu, H.H. Wu, S.F. Liu, J.G. Tang, M. Zhou, H. Wang, et al., Effects of stacking fault energy on the deformation behavior of CoNiCrFeMn high-entropy alloys: a molecular dynamics study, Appl. Phys. Lett. 119 (2021) 201907.
- [42] M.C. Ha, J.M. Koo, J.K. Lee, S.W. Hwang, K.T. Park, Tensile deformation of a low density Fe-27Mn-12Al-0.8C duplex steel in associate with ordered phases at ambient temperature, Mater. Sci. Eng. A 586 (2013) 276–283.
- [43] L. Wang, J. Teng, P. Liu, A. Hirata, E. Ma, Z. Zhang, X. Han, Grain rotation mediated by grain boundary dislocations in nanocrystalline platinum, Nat. Commun. 5 (2014) 4402.
- [44] G.J. Tucker, J.A. Zimmerman, D.L. McDowell, Shear deformation kinematics of bicrystalline grain boundaries in atomistic simulations, Model. Simul. Mater. Sci. Eng. 18 (2010) 015002.
- [45] Y. Guo, D.M. Collins, E. Tarleton, F. Hofmann, A.J. Wilkinson, T.B. Britton, Dislocation density distribution at slip band-grain boundary intersections, Acta Mater. 182 (2020) 172–183.
- [46] G.J. Tucker, S. Tiwari, J.A. Zimmerman, D.L. McDowell, Investigating the deformation of nanocrystalline copper with microscale kinematic metrics and molecular dynamics, J. Mech. Phys. Solids 60 (2012) 471–486.
- [47] Q. Fang, Z. Huang, L. Li, Z. Huang, B. Liu, Y. Liu, J. Li, P.K. Liaw, Modeling the competition between solid solution and precipitate strengthening of alloys in a 3D space, Int. J. Plast. 149 (2022) 103152.
- [48] Y. Guan, Y. Wang, W. Song, Modulating mechanical performances of metallic amorphous materials through phase gradient, Int. J. Mech. Sci. 234 (2022) 107680
- [49] F. Zhang, K. Liu, Q. Tang, G. Li, D. Zhu, Simulation study on the nano-crystalline Cu-Ag alloys with gradient segregation, Mater. Lett. 330 (2023) 133395.